




OPEN

Cefotaxime removal enhancement via bio-nanophotocatalyst α -Fe₂O₃ using photocatalytic degradation technique and its echo-biomedical applications

Mostafa F. Al-Hakkani^{1,2}, Gamal A. Gouda¹, Sedky H. A. Hassan^{3,4}, Mohammed S. Saddik⁵, Mohamed A. El-Mokhtar⁶, Maggie A. Ibrahim⁶, Mahmoud M. A. Mohamed² & Adham M. Naguib¹

The present paper evaluates the photocatalytic degradation (PCD) performance of the biofabricated hematite nanoparticles (α -HNPs) for the degradation approach of the Cefotaxime (Cfm). The optimum pH of the solution to achieve the best PCD was found to be 10.5. The kinetics study for the PCD of the Cfm via α -HNPs has been investigated and the reaction was found to be fellow pseudo-first-order at $R^2 = 0.992$. The mass loading impact of α -HNPs was investigated and estimated for the maximum degradation of Cfm 0.4 mg/mL. UV-Vis confirmed that α -HNPs had a direct transition bandgap at 3.78 eV at a maximum absorption wavelength of 362 nm with suspension stability for 7 days. The probable mechanism of the Cfm PCD via α -HNPs and the degradation pathway was conducted. The validation of the suspension stability of the α -HNPs (-68.6 ± 11.8 mV) was determined using the zeta potential investigation test. XRD investigation was conducted after Cfm PCD showing an average crystallite size of 27.0 nm. XRD, TEM, SEM, EDX, and FT-IR analyses have been conducted for the α -HNPs before and after Cfm PCD confirming the high efficiency for the reusability of the current biocatalyst α -HNPs for further use. TEM results of the particle sizes of α -HNPs were found at 19.2 ± 4.4 and 20.6 ± 7.4 nm respectively before and after Cfm PCD. The efficiency of the Cfm PCD was found to be 99.1% after 6 h. High potent as an antibacterial agent of α -HNPs was investigated either α -HNPs alone or after its PCD activity against Cfm. The antibacterial activity revealed high sensitivity, especially toward Gram-positive species indicating its promising ability against pathogenic issues. Interestingly, Cfm@ α -HNPs showed superior anti-proliferative activity as tested by MTT assay and were able to induce apoptosis in MCF7 and HepG2 cell lines using the flow cytometry technique at 20.7% and 17% respectively. Also, The IC₅₀ of hydrogen peroxide scavenging was estimated and it was manifested that 635.8 and 665.6 μ g/mL of α -HNPs before and after the PCD process of Cfm respectively.

The necessity to treat wastewater is a critical issue in the world especially. There are several ways for water to become polluted. Contamination from dyes, pharmaceuticals, and industrial waste is one of these sources¹. Water containing organic pollutants such as industrial pharmaceutical waste and chemicals generated by textile industries has an impact on the biological cycle, specifically the photosynthesis process in plants, which has a direct impact on marine species and an indirect impact on human life². Furthermore, polluted water has a significant influence on the life of birds, animals, and humans who are impacted by contaminated flowing water³.

¹Department of Chemistry, Faculty of Science, Al-Azhar University, Assiut Branch, Assiut 71524, Egypt. ²Department of Chemistry, Faculty of Science, New Valley University, El-Kharja 72511, Egypt. ³Department of Biology, College of Science, Sultan Qaboos University, 123 Muscat, Oman. ⁴Department of Botany and Microbiology, Faculty of Science, New Valley University, El-Kharja 72511, Egypt. ⁵Department of Pharmaceutics and Clinical Pharmacy, Faculty of Pharmacy, Sohag University, Sohag 82524, Egypt. ⁶Department of Medical Microbiology and Immunology, Faculty of Medicine, Assiut University, Assiut 71515, Egypt. ✉email: mostafa.farouk15@azhar.edu.eg

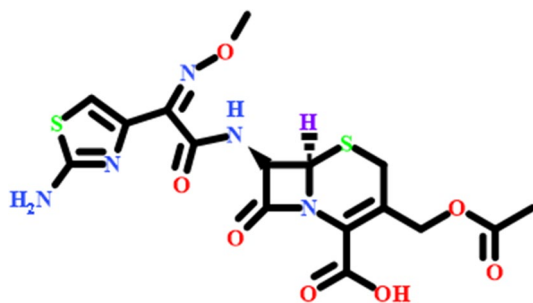


Figure 1. Structure of Cefotaxime ($C_{16}H_{17}N_5O_7S_2$); molar mass: 455.46 g/mole.

Pharmaceuticals have been broadly spectrum used in the last four decades in human, sustainable agriculture, aquaculture, and vet application areas for bacterial infection treatment especially for enhancing the quality of human life⁴. Pharmaceuticals are an emerging environmental hazard due to the extremely large use of antibiotics that can easily be found in the aqueous environment, especially those that are classified as water-soluble drug substances. These drug constituents have been observed in drinking water^{1,5,6}, surface water⁷⁻⁹, groundwater^{9,10}, and sewage effluent¹¹⁻¹³. The pharmaceutical drug substances can reach the aquatic environment via diversified sources such as pharmaceutical industrial wastewater^{1,14}, Hospital drains¹⁵, and plants for conventional wastewater treatment^{16,17}. Of the diverse pharmaceutical drug products, antibiotics have been of considerable environmental concern due to the emergence of antibiotic-resistant bacteria which couldn't be treated with currently recognized prescription, and the resulting rise in their chemical toxicity^{1,18-20}. Cefotaxime (*Cfm*) is a typical example of an antibiotic. It is classified from the cephalosporin family of beta-lactam as one of their third-generation member Fig. 1. It has an antibiotic broad-spectrum activity as an antibacterial agent against either gram-positive or gram-negative micro-organism species²¹.

Many studies reported that the *Cfm* in the effluents after the wastewater treatment of the plants, hospitals drain, and sewage treatment facilities could be detected at a concentration greater than 300 ng/L²²⁻²⁵.

Although the toxicity of *Cfm* concentration in the aquatic environment is relatively low, the augmentation of resistant bacteria and resistance genes as a result of *Cfm* use is a more immediate issue²¹. Furthermore, because of its biodegradability, *Cfm* cannot be successfully removed by usual wastewater treatment techniques. As a result, innovative alternative solutions to the antibiotic contamination problem are necessary. León et al.²⁶ reported a removal efficiency of 84.2% of 20 mg/L of *Cfm* removal photocatalytic method via 2.5 g/L of TiO_2 . Also, in a recent study mesoporous C_3N_4 was used as a photocatalyst by Mengmeng et al.²² in 1 g/L to remove the *Cfm* residual in a concentration of 2 mg/L in 60 min with an efficiency of 99%.

Several treatment approaches have been introduced to overcome this environmental issue, such as conventional methods such as biosorption, coagulation, membrane process, sedimentation, flocculation, filtration, and adsorption^{1,27-29}. Owing to the unsatisfactory efficacy and often lack of utility of these methods, modern alternative advanced oxidation processes have arisen³⁰. The later methods included different processes of chemical oxidation (O_3 , H_2O_2), photochemical (UV/ H_2O_2), and photocatalysis ($TiO_2/ZnO/UV$) that were used to generate the radical oxygen species (ROS) as hydroxyl radical ($\cdot OH$). ROS has high activity as an oxidizing agent against divers of pharmaceutical compounds that have been successfully applied³¹. However, in commercial applications, the separation and recycling of ultrafine catalysts from treated wastewater are problematic, which could also pollute the treated water and is time-consuming and costly. These issues can be overcome by immobilizing the solid support PCD, which has an outstanding capacity to isolate Nano-sized materials and is cost-effective³². There is considerable interest in the wastewater treatment approach development that inevitably involves photocatalysts based on semiconductor nanomaterials especially transition metal oxides like $BiVO_4$, WO_3 , ZrO_2 , TiO_2 , MnO_2 , Fe_2O_3 , CuO , Cu/TiO_2 , ZnO , ZnO/Sb_2MoO_6 , and $C@Cu_2O@Cu$ nanocomposite^{1,3,33-39}.

Among all of these, Alpha Hematite Nanoparticles Fe_2O_3 (α -HNPs) offers several advantages such as low-cost, chemical stability, nontoxicity, and wide band gap^{2,34}. To the best of our knowledge, we conduct herein for the first time photocatalytic of *Cfm* using α -HNPs. In this work, nanostructured α -HNPs (28.01 g/m²) were prepared as previously reported using a greener approach³⁶. The resulting α -HNPs were characterized using various characterization techniques. The objectives of this investigation are to gain a mechanistic pathway in PCD of the *Cfm* wastewater-contaminant as an antibiotic model.

Materials and methods

Chemicals and reagents. All chemicals used in the current work were analytical grade. Methanol HPLC grade from (Merck). *Cfm* standard ($C_{16}H_{17}N_5O_7S_2$); molar mass (455.46 g/mole); purity (96.3%) Zhuhai United Laboratories Co. Ltd (India) was kindly supplied by UP pharma (Assiut, Egypt). Disodium hydrogen phosphate anhydrous, Hydrochloric acid, Phosphoric acid 85%, Sodium hydroxide, and Hydrogen peroxide (Scharlau, Spain). Deionized water used in the analysis was prepared by reverse osmosis and passed through a 0.45 μm Millipore filter (Millipore Company, USA) before use.

Instrumentation. UV-vis absorption measurement of the α -HNPs absorption was recorded in the range 200–800 nm using PerkinElmer [LAMBDA 40] Spectrophotometer using a quartz cell of 1 cm path length at

room temperature. Malvern Zeta Sizer equipped with a 4mW helium/neon laser wavelength equals 633 nm at 25 °C (Nano-ZS). The XRD parameters as crystallite size “D” could be determined using the Scherrer equation for each peak. Also, the other XRD parameters could be estimated as the strain of the lattice (ϵ), placing distance (d), dislocation density (δ) and stacking fault (α), crystallinity (%), and crystallinity index (CI) as manifested in the supplementary material file; Eqs. (1–7)^{3,36,37}. FT-IR analysis was recorded on a Thermo Fisher [Nicolet iS10 FT-IR spectrometer] in a wavenumber range of 4000–400 cm^{-1} using an ATR module. The particle size of the α -HNPs before and after *Cfm* PCD was conducted using transmission electron microscopy [TEM; JEOL JEM-100C XII]. The morphology and chemical composition of the α -HNPs and *Cfm*@ α -HNPs were investigated using scanning electron microscopy [SEM; JSM IT 200]. *Cfm* quantitative analysis and its related substances were determined using the LC-20A HPLC instrument with the PDA (Shimadzu). The method was performed on the (Thermo Scientific) RP column BDS (150 mm \times 4.0 mm \times 5 μm) with a PDA detector at 235 nm, column oven at 30 °C, and injection volume of 20 μL . Flow cytometry was carried out using FACS-Calibur flow cytometer (Becton Dickinson, USA) and data were analyzed using FlowJo software (Treestar, Ashland, OR).

Methods and experiments. The photocatalytic efficiency studies were conducted under direct sunlight irradiation from 11.00 AM to 5.00 PM. All the study experiments were implemented according to the previously reported *Cfm* HPLC analysis method by Al-Hakkani²¹. As a general procedure, after any process of *Cfm* solution and α -HNPs treatments the samples were filtered using nylon filter paper with a pore size of 0.45 μm using the Buckner filtration system. Then as an assurance procedure, an additional filtration step was performed using a syringe filter of 0.2 μm before introduction to the HPLC for analysis. To identify the related substances that were produced from the *Cfm* degradation; individual impurities (A, B, C, E, and F) were injected under the same analysis circumstances according to European Pharmacopoeia^{21,40}. The resolution between the nearest adjacent peak and the *Cfm* principle peak should be more than 1.5 according to the guidelines of the analytical method validation protocols^{21,33,41–44}.

Batch mode experiments. The placebo samples “*Cfm* only without any processes applied as adsorption, photolysis or PCDs” were conducted as a zero time for each experiment individually for each parameter for the whole of the study. Also, samples after 2 h of adsorption in the dark under continuous stirring at 350 rpm were conducted before starting the photocatalytic study to exclude the adsorption/desorption effect.

The degradation % was calculated using the equation in the supplementary material file; Eq. (8).

Interactive effect of solution pH change. Lopez-Alvarez et al.⁴⁵ reported that the most important parameters affecting the PCD process are the pH of the solution and catalyst dose. So, both of them and the time effect parameter were to be evaluated.

The photolysis and photocatalytic studies were conducted for 6 h via direct sunlight for 250 mL of *Cfm* 20 mg/L using 250 mg of as-biofabricated α -HNPs with continuous stirring at 350 rpm. The impact of solution pH on the *Cfm* degradation was implemented firstly by maintaining all the parameters fixed at different pH medium solutions in the range (2.5–12.5). Hydrochloric acid 0.1 M and sodium hydroxide 0.1 M were used for the pH adjustment. The pH of the solution was adjusted before starting the sunlight irradiation and is not controlled while conducting the degradation reaction.

Kinetic mechanism studies. To determine the time effect “kinetic study profile”, 250 mL of *Cfm* 20 mg/L at pH 10.5 samples were prepared in a beaker containing 250 mg of the as-biofabricated α -HNPs under continuous stirring at 350 rpm. At different time intervals (1, 2, 3, 4, 5, and 6 h); the degradation % of *Cfm* was estimated.

The rate constants of the *Cfm* PCD can be estimated via the pseudo-first-order and second-order equations as in the supplementary material file; Eqs. (9,10).

Influence of the as-biofabricated α -HNPs catalyst loading. For the investigation study of the as-biofabricated α -HNPs mass on the photolysis and photocatalytic activities of *Cfm*, 250 ml of *Cfm* solution 20 mg/L at pH 10.5 samples were prepared. Solutions were taken individually in a beaker at different quantities of α -HNPs at (0.04–1.0 g/L). Then the samples were exposed to direct sunlight with continuous stirring at 350 rpm.

Practical application using an actual pharmaceutical wastewater sample after production of *Cfm*. Initially and before the photocatalytic process application, the physicochemical parameters as solution pH, conductivity, total dissolved solids (TDS), and zero-time HPLC assay were analyzed. In a 100 mL beaker; 50 mL of an actual pharmaceutical wastewater sample that was previously filtered through a nylon membrane filter of 0.45 μm , the α -HNPs were added to get a concentration of 1.0 mg/mL with continuous stirring for 2 h at 350 rpm at room temperature. Consequently, the sample was left in direct sunlight from 11:00 AM to 04:00 PM. After completion of the reaction, the sample was filtered using nylon filter paper with a pore size of 0.45 μm using the Buckner filtration system, then an additional filtration step was performed using a syringe filter of 0.2 μm before introduction to the HPLC instrument for analysis.

Antibacterial activity. Four examples were used for the investigation of the antibacterial activity of the as-prepared α -HNPs against *Cfm*@ α -HNPs after *Cfm* degradation. Gram-negative bacteria species were tested as *Escherichia coli* (*E. coli*) and *Salmonella typhimurium* (*S. typhimurium*). While *Enterococcus faecalis* (*E. faecalis*) and *Staphylococcus albus* (*S. albus*) were testes as examples of Gram-positive bacteria. The bacterial types were kindly provided by the lab of Microbiology; Faculty of Science; New Valley University, Al-kharga, Egypt. The

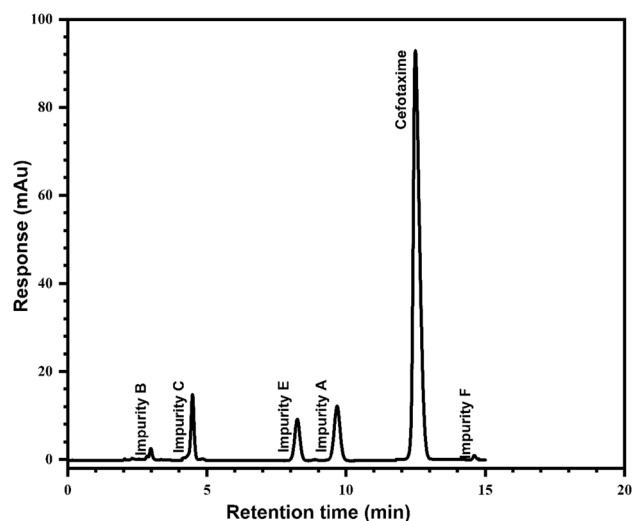


Figure 2. Cefotaxime and its related substances HPLC chromatogram.

antibacterial activity was investigated via the agar well diffusion according to Magaldi et al.^{1,46}. In brief, the wells were made by punching the nutrient agar surface with the sterile cork borer (8 mm diameter). The Dimethyl sulfoxide (DMSO) was used as a negative control where all testes were suspended in DMSO as a solvent. Cefotaxime sodium (Cephalosporin third-generation antibiotic) 250 µg/mL was used as a positive control. *Echinacea purpurea* (*E. purpurea*) and the as-prepared α -HNPs against *Cfm*@ α -HNPs after *Cfm* degradation were tested at a concentration of 1000 µg/mL. All tests were added to the wells. The Petri dishes were incubated at 30° C for 24 h, and the clear inhibition zones were estimated in mm and recorded.

Anti-proliferative activity. MTT assay was used to evaluate the effect of the different compounds on the proliferation of MCF7 cells (breast carcinoma cell line) and HepG2 cells (Human liver Hepatoma carcinoma cell line). About 5×10^4 cells were inoculated in wells of 96 well tissue culture plates. Then cells were treated with serial dilutions of the tested samples and incubated at 37° C overnight. MTT solution (Promega, USA) was applied at the recommended concentration to cells for 3 h and the formed formazan crystals were solubilized. The optical density was measured at 560 nm and the anti-proliferative activity of *E. purpurea* liquid extract, α -HNPs, and *Cfm*@ α -HNPs were evaluated against control untreated cells as previously described.

To confirm these results, MCF-7 cells were treated with the *E. purpurea* liquid extract, α -HNPs and *Cfm*@ α -HNPs at a concentration of 100 µg/ml for 24 h, and apoptotic cells were evaluated using flow cytometry. Following incubation with the indicated test samples, cells were stained with Annexin V-FITC and propidium iodide (FITC Annexin V Apoptosis Detection Kit with PI, Biolegend, USA) to evaluate the frequency of late apoptotic cells which acquired both dyes.

Hydrogen peroxide scavenging (H₂O₂) assay. The ability of as-biofabricated α -HNPs to scavenge hydrogen peroxide can be determined according to the reported method by Ruch et al.⁴⁷. A solution of 0.004 M of hydrogen peroxide was prepared using the 0.05 M phosphate buffer pH 7.4 solution as a solvent. The blank solution was conducted using a phosphate buffer solution in absence of the hydrogen peroxide. The standard hydrogen peroxide concentration was estimated spectrophotometrically via absorption measurement at 230 nm as (A_S). The as-biofabricated α -HNPs were suspended in the distilled water subsequently, they were added to the hydrogen peroxide/phosphate buffer in a final concentration range (10–1000 µg/mL). Finally, the absorbance at 230 nm was determined after 10 min as (A_T).

The scavenging percentage of hydrogen peroxide could be calculated as in the supplementary material file; Eq. (11).

Results and discussion

The retention time (R_t) of the *Cfm* peak was found to be about 12.5 min. Also, the R_t of *Cfm*-related substances was determined and found to be at about 2.9, 4.4, 8.2, 9.6, and 14.6 min for impurities B, C, E, A, and F respectively.

The *Cfm* principle peak was found to be resolved from the impurity F at an excellent value via 8.11 as revealed in Fig. 2. Any other impurity less than the reporting level at 0.05% of the *Cfm* peak area in the chromatogram will be disregarded according to the European Pharmacopoeia guideline⁴⁰.

Interactive effect of solution pH change. The pH of the solution in diverse photocatalytic systems is a factor that can affect the polarization of the catalyst and the dissociation of the substrate, which can determine the various electrostatic interactions among the present species in the reaction medium^{1,48,49}.

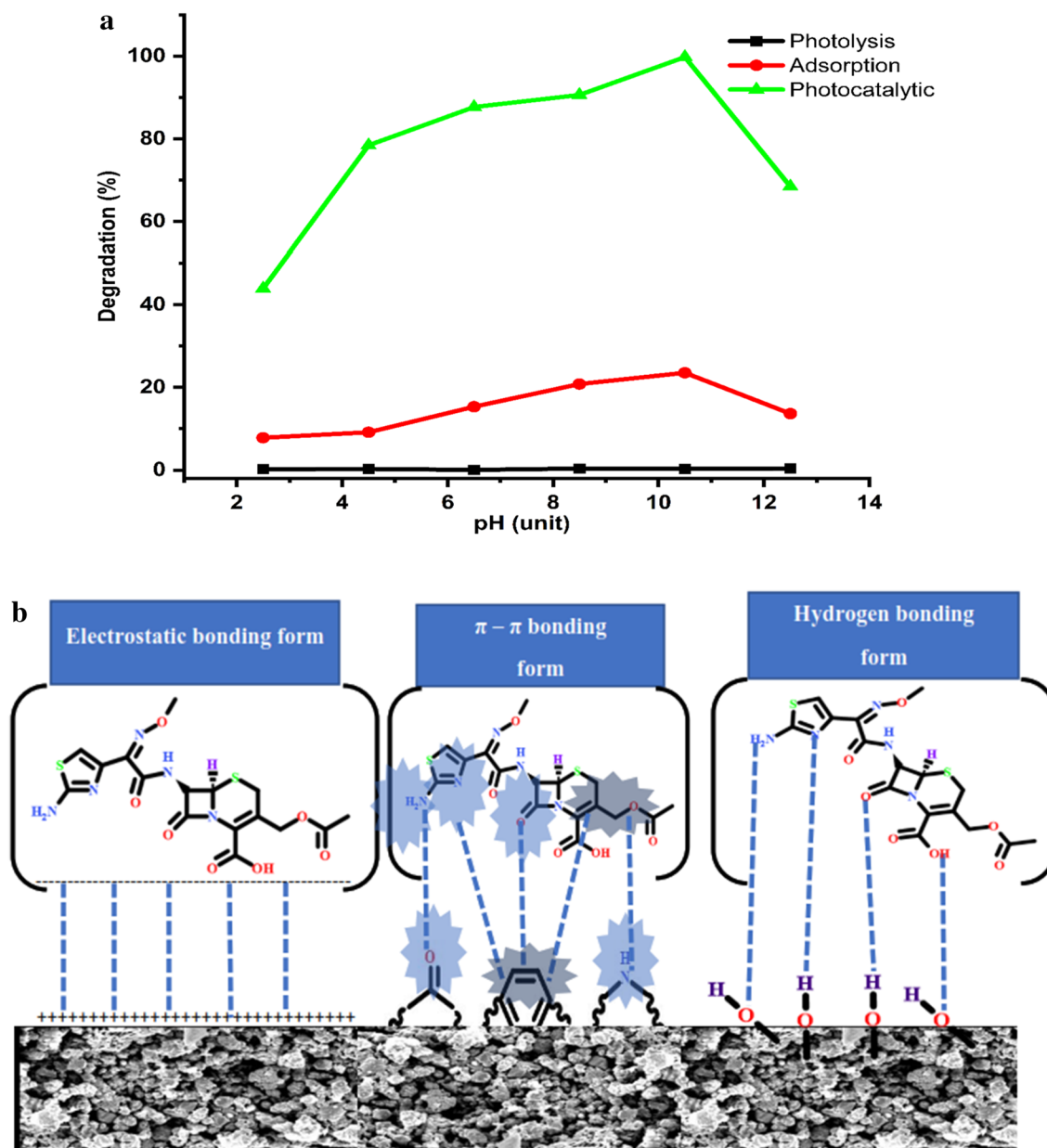


Figure 3. (a) Cefotaxime degradation (%) against pH solution change effect. (b) Cefotaxime/ α -HNPs binding form probabilities.

To study the solution pH effect on the degradation of *Cfm*; some experiments were implemented in solution pH within the range of 2.5–12.5 maintaining the rest of the experiment factors fixed at 1.0 g/L of α -HNPs loading dose and 250 mL of 20 mg/L of *Cfm* concentration for 6 h.

According to Fig. 3a; the comparison profiles for both photolysis and photocatalytic for *Cfm* degradation; it can be concluded that there is no effect of the sunlight alone on the *Cfm* degradation over at the full pH range 2.5–12.5. On the other hand, the photocatalytic of the *Cfm* degradation increased dramatically (43.9–90.6%) in the pH range 2.5–8.5 showing the maximum degradation of *Cfm* (99.8%) at pH 10.5 followed by decreasing at pH 12.5 (68.5%).

The *Cfm* degradation usually depends on the adsorption of its molecules onto the α -HNPs surface and the generation of the hydroxyl free-radical which depends on the availability of hydroxyl ions in the reaction medium. As a result of the previous determination of the zero-point charge (pH_{zpc}) of α -HNPs that was found to be 5.2³⁶. So, at the pH of solutions below this value; the α -HNPs surface will be positively charged. On the contrary, at pH solutions more than pH 5.2, the α -HNPs surface will be negatively charged. *Cfm* shows three pK_a (acid dissociation constant) values at 2.1, 3.4, and 10.9 as León et al. reported⁵⁰. So, the *Cfm* at pH range (4–10.5) presents as negatively charged ions.

According to the attraction electrostatic force among the α -HNPs surface charges and the *Cfm* ions under the dedicated pH reaction medium (2.5–4.5), the promotion to generate the hydroxyl radicals was enhanced.

The increase in *Cfm* degradation efficiency % at the pH range (6.5–10.5) may be attributed to hydrogen bonding formation between the *Cfm* and the adsorbed bioactive molecules that surrounded the as-biofabricated α -HNPs or π - π interaction^{1,36,37} as manifested in Fig. 3b.

Completely *Cfm* dissociation at pH 12.5 or more causes the presence of the *Cfm* species as deprotonated anions and the negatively charged surface of the as-biofabricated α -HNPs maybe it is the main cause of the repulsion electrostatic force. That was subsequently, followed by a decrease in *Cfm* degradation.

Kinetic mechanism studies. The *Cfm* responses at zero time, after adsorption, and after the PCD at different time intervals (1–6 h) were manifested in Fig. 4a. It is very clear that the efficacy of the as-biofabricated α -HNPs on *Cfm* degradation as a photocatalytic agent. The *Cfm* peak response was decreased rapidly as a function of degradation time.

The first rapid PCD was observed at the first hour of the reaction and it was found to be 47.2%. The increase of PCD efficiency almost reached the maximum after 4 h at (96.4%). After that, the progress in the degradation was limited where it was increased up to 97.9% followed by a slight increment at 99.1% after further 2 h of sunlight time exposure as depicted in Fig. 4b. So, the critical photocatalytic time interval is represented after 4 h of the reaction.

As the HPLC degradation profile manifested (Fig. 4c and Table 1); the *Cfm* further degradation resulted from related substances (impurities A, B, C, E, and F) showed a notable increase in their responses. The most abounded of these related degradant substances was impurity C which gave an increased assay response factor at a ratio from <0.05% at *Cfm* zero-time assay to 1.36% at the end of catalytic degradation after 6 h. Impurity A came in the second-order of the increase in its assay response by 1.32% from the *Cfm* zero-time assay. Impurities E, B, and F came posteriorly in degradation ratios assay as 1.00%, 0.27%, and 0.14% respectively.

It is clear that the total impurities assay was about 3.82% of the principle *Cfm* peak, this ratio reflects the strength of the as-biofabricated α -HNPs toward *Cfm* degradation for its primary components as carbon dioxide and water.

Figure 4d shows that the *Cfm* degradation fits appropriately with first-order kinetic according to the R^2 value which was found to be 0.992. The rate constant of the *Cfm* was found to be 0.8325 h⁻¹.

Influence of the as-biofabricated α -HNPs catalyst loading. It is clear to man that without using the α -HNPs catalyst (photolysis) there was no significant degradation change over the reaction time of 6 h and it can be neglected as shown in solution pH and time change effect.

For studying the effect of the as-biofabricated α -HNPs loading, a series of experiments were conducted for 4 h at different doses of the α -HNPs in the range 0.04 to 1.0 g/L maintaining the *Cfm* concentration at 20 mg/mL and pH of 10.5 as shown in Fig. 5.

The photocatalytic is a surface phenomenon so, it strongly depends on the crystallinity nature and the surface area “28.01 g/m² as previously reported in our approach³⁶” that is proportional directly to the mass loading of the catalyst under study. According to the increase of the as-biofabricated α -HNPs loading, along with reaction time, there was a drastic rise in the degradation rate (58.5%, 83.4%, 96.6%, and 99.6%). So, it was found to be the degradation profile is properly dose-based. The increment efficiency of degradation may be attributed to the photon absorption via the as-prepared α -HNPs that cause the generation of the hole-electron pairs¹. So, the total activated surface area increased with increasing the catalyst dose which subsequently, increase the reactive oxygen species production as revealed in the photocatalytic degradation mechanism scheme equations. Any increase in the α -HNPs after 0.4 g/L loadings had no notable effect on the increase of *Cfm* degradation efficiency compared with the loading dose effect at (0.04–0.2 g/L). So, it can be negligible because it was an almost slight increase. This behavior may be due to the agglomeration of NPs, solution opacity, or scattering of the light at higher doses of the as-prepared α -HNPs⁵¹. So, 0.4 g/L can be selected as a convenient dose for further studies.

Photocatalytic activity comparison studies of the biosynthesized α -HNPs. From the last decade and up to date, the biofabricated α -HNPs via various parts of different kinds of plants were paid attention to and gained great interest in several applications, especially in photocatalytic activity against some of the organic substances as reported in Table 2.

UV-Vis analysis. The optical characterizations of the biosynthesized α -HNPs powder sample were investigated after it was dispersed in deionized water. The α -HNPs exhibited the maximum absorption peak in the UV range at 362 nm Fig. 6a, this result was found to be compatible with the previously reported surface plasmon (SPR) peaks by Rajiv et al.⁶⁰ and Al-Hakkani et al.³⁶. The stability of the α -HNPs suspension form in the deionized water was tested for one week by examining for the distinct SPR peak in the optical spectrum and it was found to be at the same wavelength. The bandgap energy of the as-prepared α -HNPs could be determined using the optical as manifested in the supplementary material file; Eqs. (12, 13)³. The E_g of the direct transition was estimated by extrapolating the linear portion of the plot of $(ah\nu)^2$ against $h\nu$ Fig. 6b. E_g was found to be 3.78 eV which was agreed with the previous findings by Al-Hakkani et al.³⁶ and Sharma et al.⁶¹.

Zeta potential. The suspension stability of the α -HNPs could be estimated using the value of the zeta potential instrument^{3,36}. The value of zeta potential of α -HNPs suspension stability in water was found to be -68.6 ± 11.8 mV which indicated that NPs had an excellent stability Fig. 7.

Zeta potential result was found to be compatible with the UV-Vis. α -HNPs suspension stability. Several studies reported that the colloidal/suspended particles had good stability if their charged surface passed the critical value ± 30 mV. Table 3 shows the relationship between the zeta potential value of the colloidal/suspended material

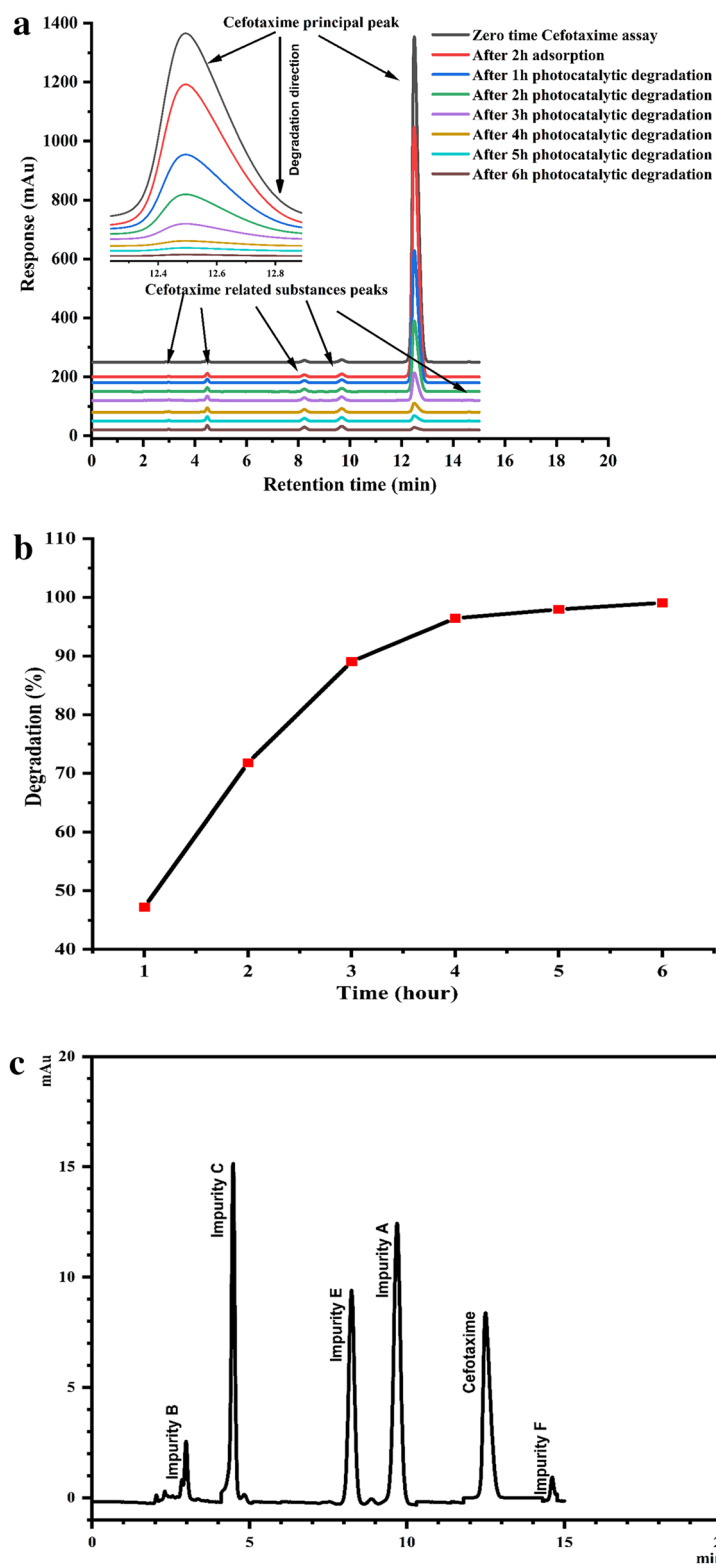


Figure 4. (a) Cefotaxime degradation (%) against different time intervals using α -HNPs. (b) Cefotaxime degradation (%) profile as a function in time. (c) Cefotaxime photocatalytic degradation after six hours via α -HNPs (HPLC-related substances profile). (d) Kinetic models I) Pseudo-first-order, II) Second-order.

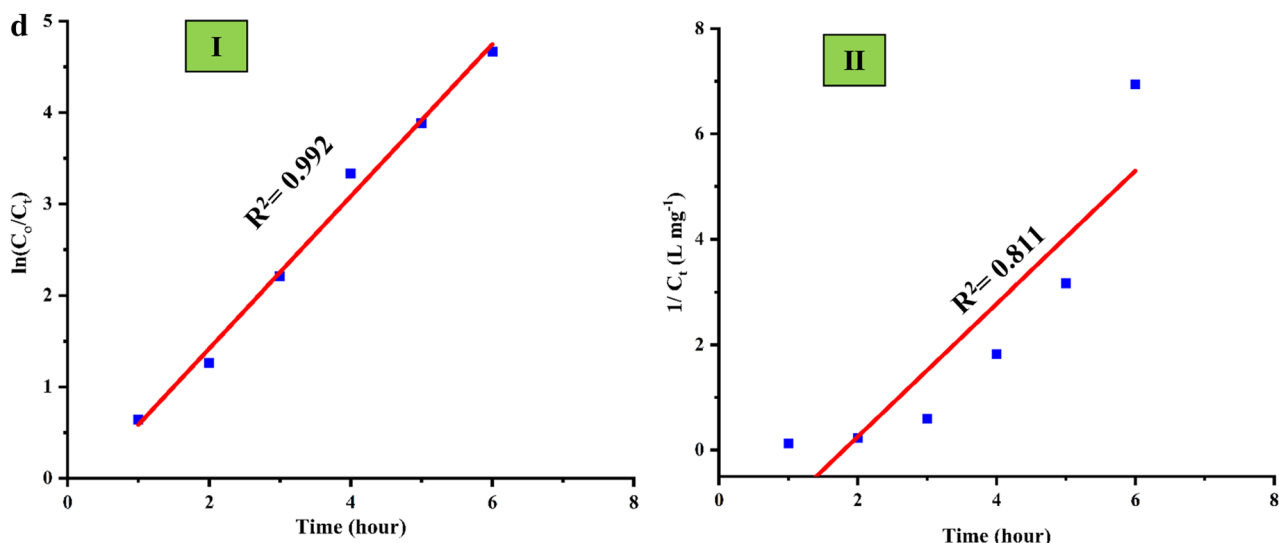


Figure 4. (continued)

Impurity	IUPAC Name	Chemical name	Molecular formula	Molar mass (g/mol)	R _i (min)	Degradation (%)
A	(6R,7R)-7-((Z)-2-(2-aminothiazol-4-yl)-2-((methoxyd3)imino)acetamido)-3-(methoxymethyl)-8-oxo-5-thia-1-azabicyclo[4.2.0]oct-2-ene-2-carboxylic acid	Cefetamet	C ₁₄ H ₁₅ N ₅ O ₅ S ₂	397.43	9.601	1.32
B	(6R,7R)-7-[[[(2Z)-2-(2-aminothiazol-4-yl)-2-(methoxyimino)acetyl]amino]-3-(hydroxymethyl)-8-oxo-5-thia-1-azabicyclo [4.2.0]oct-2-ene-2-carboxylic acid	Deacetyl Cefotaxime	C ₁₄ H ₁₅ N ₅ O ₆ S ₂	413.43	2.934	0.27
C	(6R,7R)-3-[(acetyloxy)methyl]-7-[[[(2Z)-2-[2-(formylamino)thiazol-4-yl]-2-(methoxyimino)acetyl]amino]-8-oxo-5-thia-1-azabicyclo [4.2.0]oct-2-ene-2-carboxylic acid	N-Formylcefotaxime	C ₁₇ H ₁₇ N ₅ O ₈ S ₂	483.48	4.458	1.36
E	(5aR,6R)-6-[[[(2Z)-2-(2-aminothiazol-4-yl)-2-(methoxyimino)acetyl]amino]-5a,6-dihydro-3H,7H-azeto[2,1-b]furo[3,4-d][1,3]thiazine-1,7(4H)-dione	Deacetylcefota-xime Lactone	C ₁₄ H ₁₃ N ₅ O ₅ S ₂	395.41	8.272	1.00
F	(6R,7R)-3-[(acetyloxy)methyl]-7-[[[(2Z)-2-[[[(6R,7R)-7-[[[(2Z)-2-(2-aminothiazol-4-yl)-2-(methoxyimino)acetyl]amino]-2-carboxy-8-oxo-5-thia-1-azabicyclo[4.2.0]oct-2-en-2-yl]methyl]amino]thiazol-4-yl]-2-(methoxyimino)acetyl]amino]-8-oxo-5-thia-1-azabicyclo[4.2.0]oct-2-ene-2-carboxylic acid (Cefotaxime Dimer	C ₃₀ H ₃₀ N ₁₀ O ₁₂ S ₄	850.88	14.649	0.14

Table 1. HPLC *C_{fm}* related substances impurities profile data after six hours of PCD via α -HNP_s.

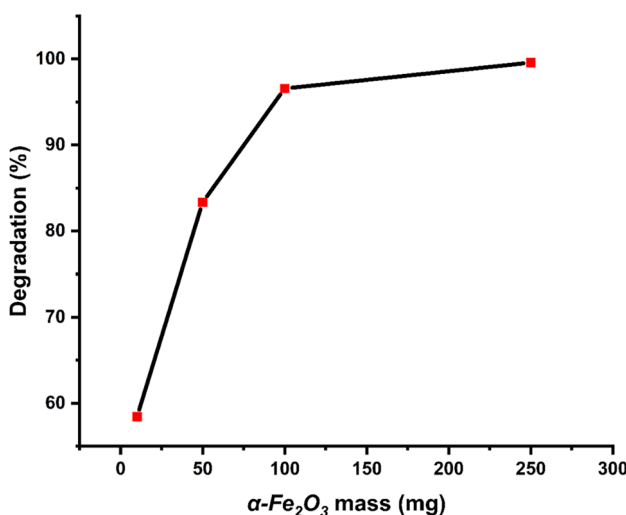


Figure 5. Cefotaxime degradation (%) against adsorbent of α -HNP_s mass effect.

Plant name/part	Substrate	References
<i>Amaranthus dubius</i> leaf	Methylene orange dye	52
<i>Cyperus rotundus</i> L.	Congo red dye	53
<i>Curcuma</i> Tea leaves	Methyl orange dye	54
<i>Cynometra ramiflora</i> fruit	Methylene blue dye	55
Pomegranate (<i>Punica granatum</i>) seeds	Blue 4 dye	56
Mandarin peels " <i>Citrus reticulum</i> "	Basic Maxilon Blue GRL, acidic Neolan Blue 2G dyes, and 2,6-dichlorophenol	57
<i>Cynometra ramiflora</i>	Rhodamine-B dye	58
<i>Carica papaya</i> leaf	Remazol yellow RR dye	59
<i>E. purpurea</i>	Cefotaxime	Current study

Table 2. Photocatalytic activity of the biosynthesized α -HNPs via various parts of different kinds of plants.

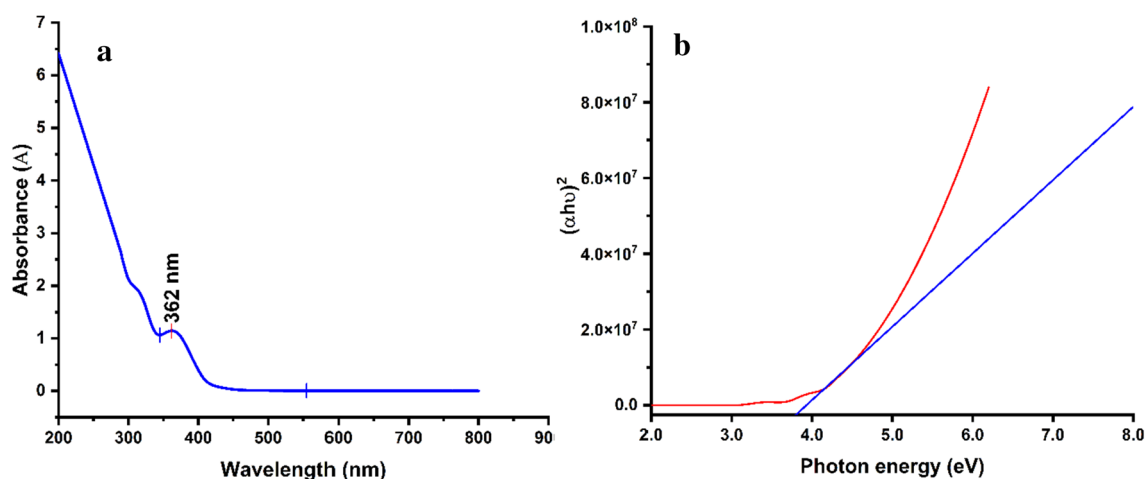


Figure 6. Spectra of the as-biofabricated α -HNPs (a) UV-Vis excitation absorption, (b) Tauc plot of direct transition energy bandgap.

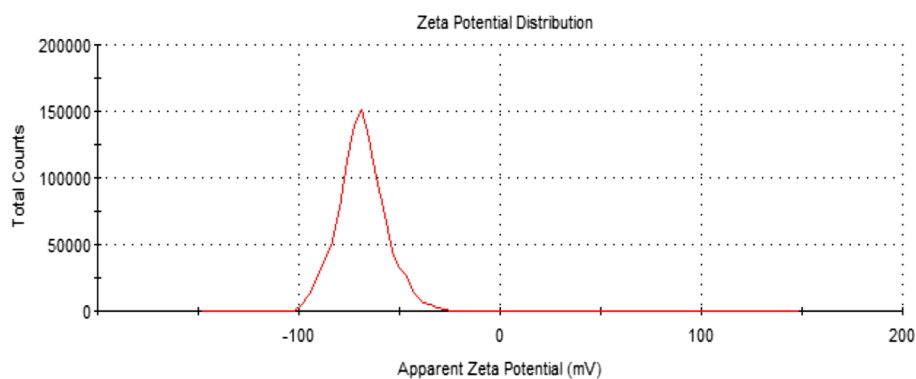


Figure 7. Zeta potential of the as-biofabricated α -HNPs.

and its corresponding relative stability. Highly positive or negative values onto the charged surface generate major repulsion forces, whilst repulsion between particles with the same electrical charge inhibits the particle agglomeration and hence it gives good dispersibility^{1-3,36,62,63}.

Degradation mechanism. Sunlight irradiation-induced α -HNPs for production of the ROS especially hydroxyl radical and superoxide anion that is mainly responsible for *Cfm* degradation. The probable degradation mechanism can be illustrated in Fig. 8.

Zeta potential value (-mV)	Colloidal/suspension stability indication	Zeta potential value (+mV)
-10, ..., 0	Flocculation or rapid coagulation	0, ..., +10
-30, ..., -10	Relative (onset)	+10, ..., +30
-40, ..., -30	Moderate	+30, ..., +40
-60, ..., -40	Good	+40, ..., +60
< -60	Excellent	> +60

Table 3. Zeta potential value stability indications.

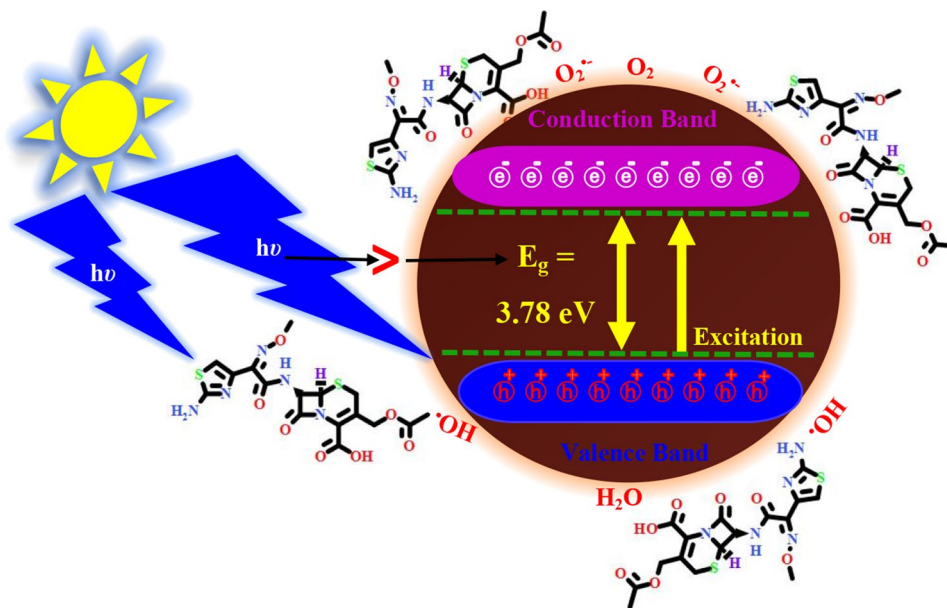


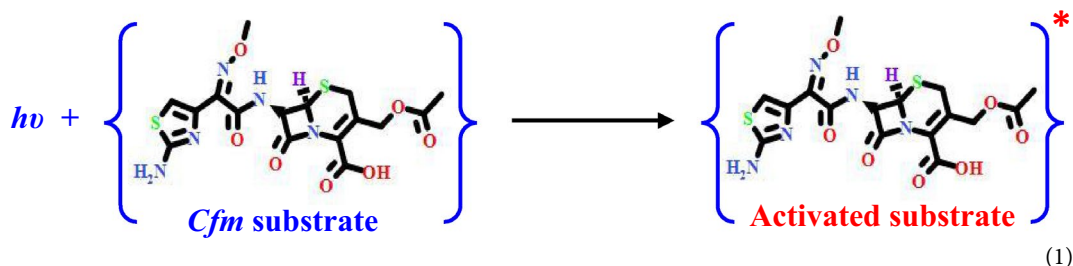
Figure 8. The Cefotaxime photocatalytic degradation probable mechanism via α -HNPs.

According to the smallest energy band gap of the as-biofabricated semiconductor α -HNPs (3.78 eV) and also as a previously reported³⁶, it can be easily excited via direct sunlight in the visible range and this is the main cause of the NPs photocatalytic activity as summarized in photocatalytic degradation mechanism scheme Eqs. (1–15). Briefly, when most of the NPs were irradiated under the sunlight induction, the electrons were being promoted to the highest energy level leaving the valence band. The hole-electron pairs were being generated; holes occupy the valence band while electrons locate in the conduction band³³.

Firstly, the holes (h^+) cause hydrolysis of water molecules to protons and hydroxyl ions which are subsequently, converted to hydroxyl radical. The ROS as hydroxyl radical considers the motive force in the oxidation of organic compounds where it acts as an oxidizing agent under convenient conditions. The final photocatalytic products are the primary components of any organic substances; that may undergo further degradation resulting water, carbon dioxide, and inorganic anions.

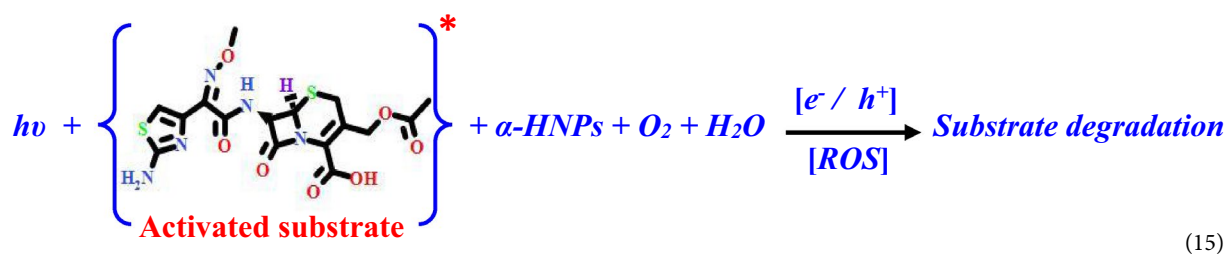
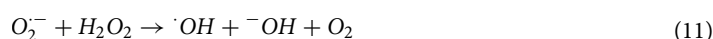
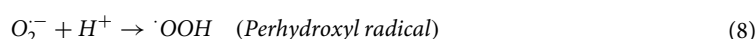
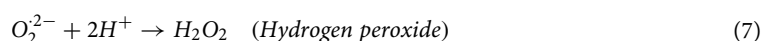
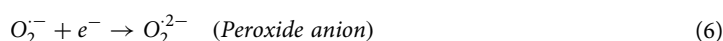
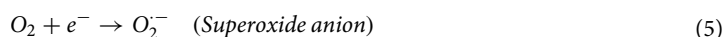
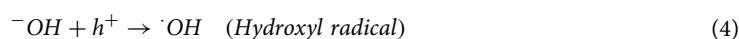
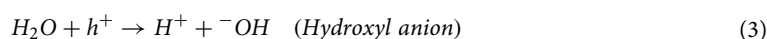
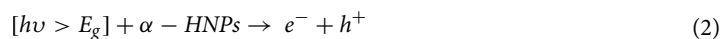
On the other hand, the negative charges (e^-) that are present in the conduction band induce the conversion of the adsorbed oxygen gas molecules to superoxide radicals which may directly degrade the organic substance or combined with the protons or holes forming an active hydroxyl radical species again and peroxides⁵⁷. Finally, we can report that the various bioactive molecules present in the *Echinacea* extract which adsorbed at the NP's surface, and the NPs themselves act as catalysts to promote photocatalytic activity.

The formation/elimination probabilities of the ROS during the PCD mechanism of *Cfm* via α -HNPs can be explored as the following mechanism scheme Eqs. (1–15):



Characteristic parameter	Before	After
Concentration (mg/L)	9.7	Not detected
Conductivity ($\mu\text{S}/\text{cm}$)	266.4	98.0
TDS (mg/L)	131.0	44.2
pH	8.16	6.81

Table 4. Water physicochemical characteristics and assay of the *Cfm*.



Cfm PCD mechanism can be summarized as shown in scheme Eq. (15); firstly, an interaction of the *Cfm* with the photon energy forms an intermediated activated substrate. Subsequently, the latter can interact with any of the ROS final species as $\text{O}_2/\text{O}_2^{\cdot-}/\cdot\text{OH}$ producing preoxylated or hydroxylated intermediate products that followed via degradation to the primarily related byproducts.

Practical application using an actual pharmaceutical wastewater sample after production of *Cfm*. Water physicochemical characteristics and assay of the *Cfm* before and after photocatalytic process activity were evaluated and listed in Table 4.

The operating procedures revealed the efficiency of the photocatalytic activity in the industrial pharmaceutical wastewater treatment using $\alpha\text{-HNPs}$ as a promising photocatalytic agent.

XRD analysis. The XRD diffractogram evidenced the highly crystalline form of $\alpha\text{-HNPs}$ after *Cfm* PCD by the Bragg's reflection peaks 2θ value and it corresponds to the lattice planes as manifested in Table 5. The dif-

2 θ ° Reference	2 θ ° _{hkl} Measured	Miller indices			D nm	ϵ nm	δ lines/nm ²	α	d Reference	d Calculated
		h	k	l					nm	nm
24.1525	24.13781	1	0	-2	28.3	5.9×10^{-3}	1.2×10^{-3}	2.7×10^{-3}	3.6818	3.6871
33.1636	33.18749	1	0	4	29.0	4.2×10^{-3}	1.2×10^{-3}	2.3×10^{-3}	2.6991	2.6994
35.636	35.65609	2	-1	0	28.3	4.0×10^{-3}	1.2×10^{-3}	2.3×10^{-3}	2.5173	2.5180
39.2899	39.2853	0	0	6	27.6	3.7×10^{-3}	1.3×10^{-3}	2.3×10^{-3}	2.2912	2.2934
40.8679	40.90785	2	-1	3	31.9	3.1×10^{-3}	9.8×10^{-4}	1.9×10^{-3}	2.2063	2.2061
43.5155	43.39244	2	0	2	20.5	4.6×10^{-3}	2.4×10^{-3}	2.9×10^{-3}	2.078	2.0853
49.4705	49.52775	2	0	-4	31.0	2.7×10^{-3}	1.0×10^{-3}	1.8×10^{-3}	1.8409	1.8404
54.0788	54.12368	2	-1	6	29.0	2.6×10^{-3}	1.2×10^{-3}	1.9×10^{-3}	1.6944	1.6945
57.6082	57.63186	1	0	-8	20.5	3.5×10^{-3}	2.4×10^{-3}	2.6×10^{-3}	1.5987	1.5994
62.4444	62.56671	3	-1	4	24.6	2.7×10^{-3}	1.7×10^{-3}	2.1×10^{-3}	1.486	1.4846
64.0089	64.09551	3	0	0	28.8	2.3×10^{-3}	1.2×10^{-3}	1.8×10^{-3}	1.4534	1.4528
69.6047	69.91427	2	0	8	15.9	3.8×10^{-3}	3.9×10^{-3}	3.2×10^{-3}	1.3496	1.3455
71.9605	72.0675	1	0	10	24.4	2.4×10^{-3}	1.7×10^{-3}	2.1×10^{-3}	1.3111	1.3105
75.4704	75.55316	4	-2	0	33.0	1.7×10^{-3}	9.2×10^{-4}	1.5×10^{-3}	1.2586	1.2585
77.7497	77.81803	3	0	-6	32.5	1.7×10^{-3}	9.5×10^{-4}	1.5×10^{-3}	1.2273	1.2274
Average	-	-	-	-	27.0	3.3×10^{-3}	1.6×10^{-3}	2.2×10^{-3}	-	-

Table 5. XRD parameters of the α -HNPs after Cefotaxime photocatalytic degradation.

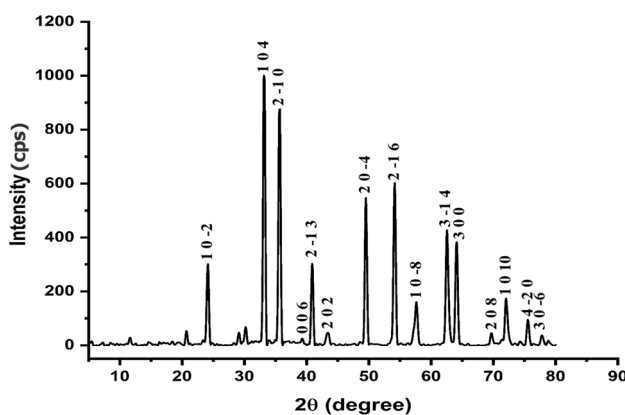


Figure 9. XRD diffractogram of the α -HNPs after Cefotaxime photocatalytic degradation.

Parameter	Before	After
Crystallite size average (D) nm	25.1	27.0
Strain average (ϵ)	4.0×10^{-3}	3.3×10^{-3}
Dislocation density average (δ) lines/nm ²	1.6×10^{-3}	1.6×10^{-3}
Staking faults average (α)	2.5×10^{-3}	2.2×10^{-3}
Crystallinity (%)	78.8%	78.7%
Reference	Al-Hakkani et al. ³⁶	Current study

Table 6. XRD parameters comparison of the α -HNPs before and after Cefotaxime photocatalytic degradation.

fraction of the peaks reflected the presence of Trigonal (hexagonal axes) of hematite crystal with $a = 5.0346 \text{ \AA}$; $c = 13.7473 \text{ \AA}$ which is identical to the reference card ICDD No: 00-901-5964. These results are compatible with our earlier study Al-Hakkani et al.³⁶ who reported the greener synthesis of α -HNPs highly crystalline as sharpness peaks depicted in Fig. 9 with the evidence of lattice plans. Any other presence peaks may be attributed to the Cfm or their related substances from the adsorption process and/or Cfm PCD onto the surface of α -HNPs^{1,2}. A slight increase of the average crystallite size (D) 27.0 nm after the Cfm PCD indicates the high efficacy of the reusability of the bio-nanocatalyst α -HNPs for further use. Table 6 shows a comparison of the XRD parameters for the α -HNPs before and after Cfm PCD.

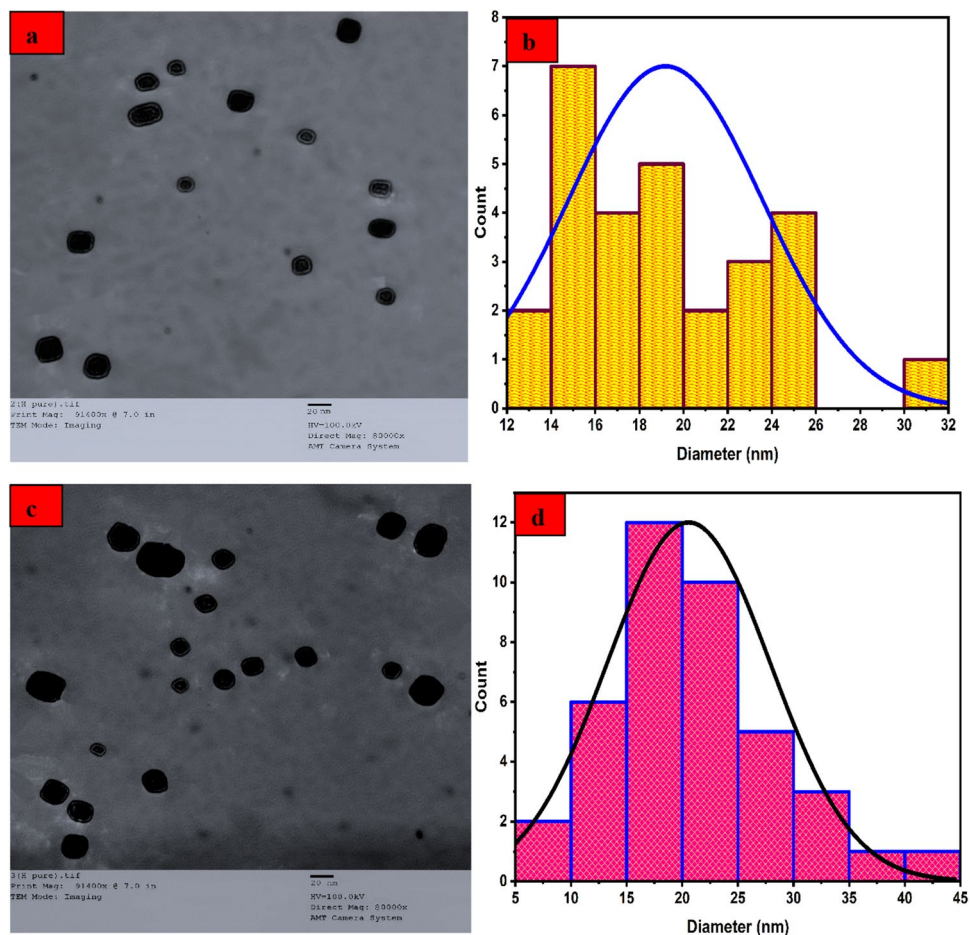


Figure 10. TEM analysis and particle distribution of α -HNPs before (a, b), after (c, d) Cefotaxime photocatalytic degradation.

Item	Before	After
Average particle sizes (nm)	19.2	20.6
Standard deviation (nm)	4.4	7.4
Minimum particle size (nm)	12.6	6.3
Maximum particle size (nm)	30.2	40.4
Median (nm)	18.8	19.8
Crystallinity index (CI)	1.1	0.71
Crystallinity nature	Monodispersed	

Table 7. TEM analysis of α -HNPs before and after *Cfm* PCD.

TEM analysis. The α -HNPs before and after *Cfm* PCD TEM analysis were being investigated as depicted in Fig. 10. Although there is an obvious very little increase in some of the particles which may be attributed to the adsorption process that was done before the degradation, but without any significant increment in particle sizes.

Monodispersed cubic shapes were being manifested without any signs of particle agglomeration. The statistical calculations of the corresponding analysis were introduced in Table 7.

It's clear to the man there is no change in the particle sizes of the α -HNPs before and after the *Cfm* photocatalytic process. This is an indication of the validity of α -HNPs for use to further run again without any significant change in the α -HNPs efficiency.

Morphological and chemical composition analysis (SEM and EDX). The surface morphology of α -HNPs before and after *Cfm* PCD was introduced as shown in Fig. 11. It's clear and easy for man the distinguish the surface's nature and changes that have been happened for each case of α -HNPs. EDX analysis showed a stronger proof

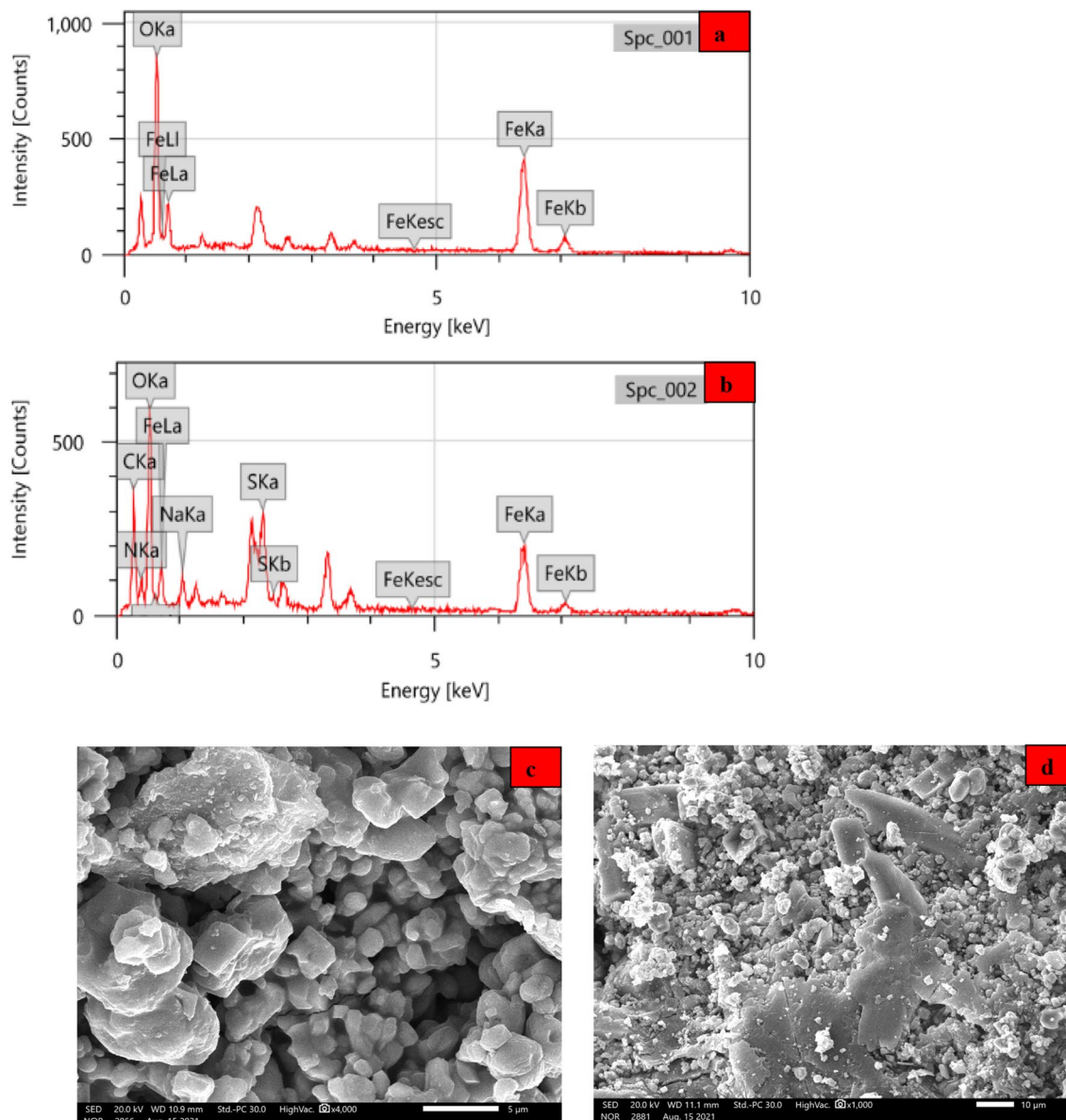


Figure 11. α -HNPs before and after Cefotaxime photocatalytic degradation EDX analysis (a, b); SEM analysis (c, d).

to differentiate between α -HNPs elemental composition alone and α -HNPs after implementing the *Cfm* PCD process. EDX analysis in the case of α -HNPs without any treatment process manifested that the main element components are only oxygen and iron atoms Fig. 11A. While after the *Cfm* PCD process that occurred at the surface of the α -HNPs Fig. 11B we can see other elements that have appeared as carbon, nitrogen, sodium, and sulfur that are the main composition of *Cfm* and their degradation substances as it was manifested in Table 1. This result confirms the adsorption and degradation process of *Cfm* and its related substances at the α -HNPs surface. Also, SEM analyses for α -HNPs before and after the *Cfm* PCD process have been conducted showing an observable change as Fig. 11C revealed. Some of the particles are different in shapes that appeared as light-colored plates from the original dark-colored base of α -HNPs Fig. 11D. These white plates could be attributed to the adsorption or degradation process of *Cfm* or their related substances at the α -HNPs surface.

FT-IR analysis. FT-IR analysis plays an important role to affirm the functional groups' encapsulation that adsorbed/adhered at the α -HNPs surface Fig. 12². There are some little functional groups dedicated to *Cfm* that have clear contributions from the adsorption process at the surface of α -HNPs or some of the adsorbed degradant substances from *Cfm* molecules. This was exhibited especially in the fingerprint region of *Cfm* (2000–500 cm^{-1}) except in the Fe–O band (522 cm^{-1})^{1,36}. This investigation assures the efficacy of α -HNPs that could be used for multiple photocatalytic runs and this result was found to be compatible with the previously TEM findings.

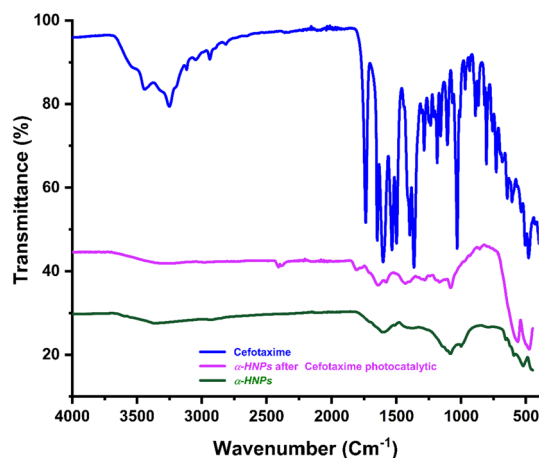


Figure 12. FT-IR analysis of Cefotaxime, α -HNPs before and after Cefotaxime photocatalytic degradation.

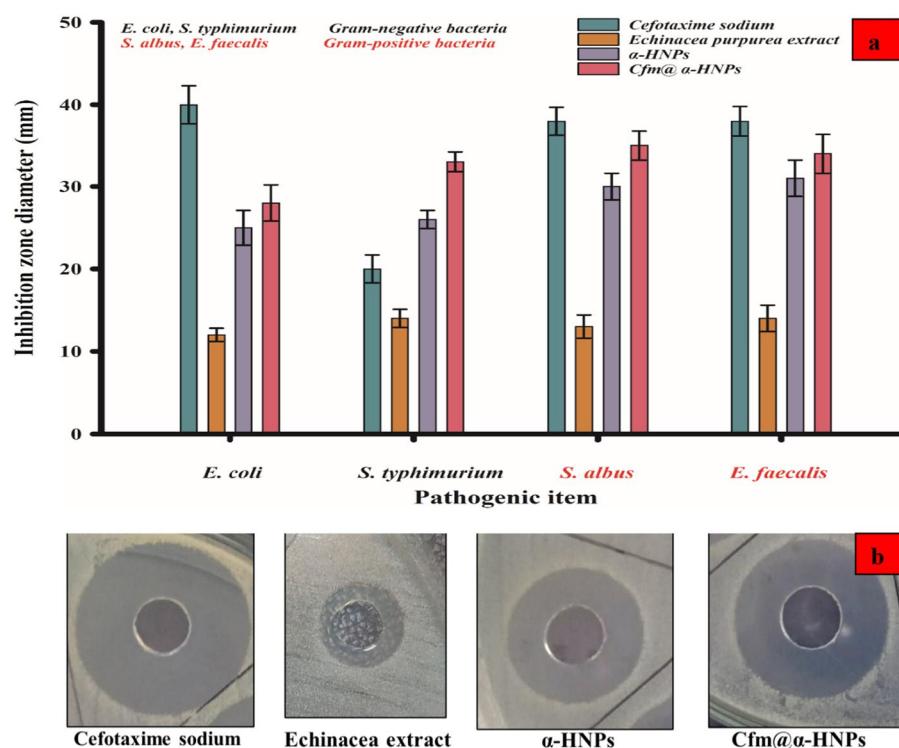


Figure 13. The antibacterial activity of (a) *E. purpurea* extract, α -HNPs before and after Cefotaxime photocatalytic degradation using Cefotaxime sodium as a positive control, (b) Representative agar diffusion showing inhibition zone diameters of the different treatments on *S. albus*.

Antibacterial activity. Results showed that DMSO had no antibacterial effect where there are no clear zones appeared. On the contrary, the aqueous extract of *E. purpurea* exhibited a moderate antibacterial activity almost was the same against both the Gram-positive and Gram-negative bacteria in the range of clear zone 12–14 mm. On the right-hand Cefotaxime manifested more activity against all tested bacterial species. The clear zones against *E. coli*, *S. albus*, and *E. faecalis* were found to be 40, 38, and 38 mm respectively where it showed a clear zone of 20 mm against *S. typhimurium*. The as-prepared Cfm@ α -HNPs system exhibited an antibacterial activity better than α -HNPs alone against all tested bacterial types especially for Gram-positive bacteria more than Gram-negative bacteria.

The measurements of the inhibition clear zones were depicted in Fig. 13. The difference in the clear zones in the antibacterial activity depends on the bacterial species' ability. The results indicate that the Gram-positive bacteria are more sensitive to α -HNPs and Cfm@ α -HNPs compared to Gram-negative bacteria. This could be explained by the high ability of the as-prepared NPs to penetrate the cell wall of Gram-positive bacteria. The

Plant name/part	Application	References
<i>Cynometra ramiflora</i>	<i>E. coli</i> & <i>S. epidermidis</i>	58
<i>Carica papaya</i> leaf	<i>Klebsiella</i> spp., <i>E. Coli</i> , <i>Pseudomonas</i> spp. & <i>S. aureus</i>	59
<i>Sida cordifolia</i>	<i>B. subtilis</i> , <i>S. aureus</i> , <i>E. coli</i> & <i>K. pneumonia</i>	64
<i>Lantana camara</i> leaf	<i>P. aeruginosa</i>	60
<i>Terminalia bellirica</i> ; <i>Moringa oleifera</i> fruit & <i>Moringa oleifera</i> leaves	<i>S. aureus</i> , <i>B. subtilis</i> & <i>P. aeruginosa</i>	65
<i>Skimmia Laureola</i> leaf	<i>R. solanacearum</i>	66
Henna (<i>Lawsonia inermis</i>) leaf	<i>S. aureus</i> & <i>S. typhimurium</i>	67
<i>Rheum emodi</i> root	<i>E. coli</i> & <i>S. aureus</i>	61
<i>Laurus nobilis</i> L	<i>L. monocytogenes</i>	68
<i>E. purpurea</i>	<i>E. coli</i> , <i>S. albus</i> , <i>E. faecalis</i> & <i>S. typhimurium</i>	Current study

Table 8. Antibacterial activity of the biosynthesized α -HNPs via various parts of different kinds of plants.

Tested product	Cell line IC ₅₀ (μ g/ml)		References
	MCF7	HepG2	
<i>E. purpurea</i>	679.2	643.4	Al-Hakkani et al. ³⁶
α -HNPs	141.6	198.2	
<i>Cfm</i> @ α -HNPs	105.31	117.33	Current study

Table 9. Summary of IC₅₀ of the different tested samples on the proliferation rate of MCF7 and HepG2 cell lines.

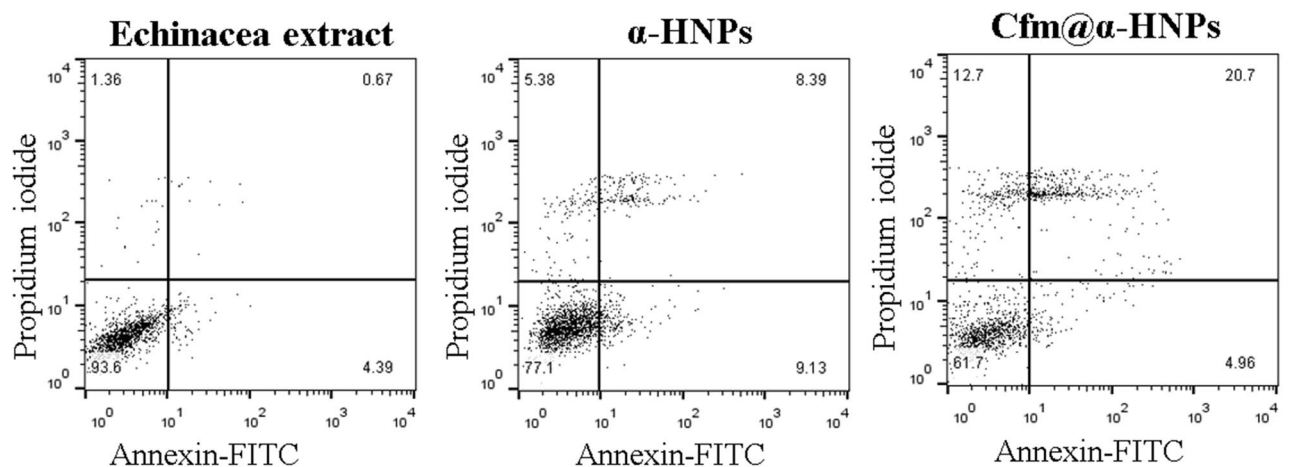


Figure 14. *Cfm*@ α -HNPs have a marked anti-proliferative activity. MCF7 cells were treated with indicated samples and the frequency of late apoptotic cells was determined using flow cytometry.

high activity of the *Cfm*@ α -HNPs compared with α -HNPs alone may be attributed to the adsorption of some of the degradation substances after the *Cfm* PCD process that are deposited onto the α -HNPs surface and they have antibacterial activity. The following comparison in Table 8 showed different antibacterial activities of green biosynthesized α -HNPs using different plant extracts.

Anti-proliferative activity. Interestingly, in addition to the antibacterial activity, the biofabricated noncompounds exhibited enhanced antiproliferative activities. IC₅₀ against MCF7 cells decreased from 679.2 μ g/ml when applying the plant extract to 105.31 μ g/ml when *Cfm*@ α -HNPs were used, pointing to marked anti-proliferative activity even compared to α -HNPs alone (IC₅₀ = 141.6 μ g/ml). A similar effect was observed using the HepG2 cells as shown in Table 9.

To confirm the results of the MTT assay, cells were incubated with 100 μ g/ml of plant extract, α -HNP, or *Cfm*@ α -HNPs and the frequency of apoptotic cells was determined by flow cytometry. MCF7 cells treated with *Cfm*@ α -HNPs showed the highest levels of apoptosis (20.7%) compared to cells treated with plant extract (0.67%) or α -HNP (8.39%) Fig. 14. Similar results were observed when HepG2 cells were tested. *Cfm*@ α -HNPs and α -HNPs induced apoptosis in 17% and 7% of cells, respectively, while cells treated with the plant extract

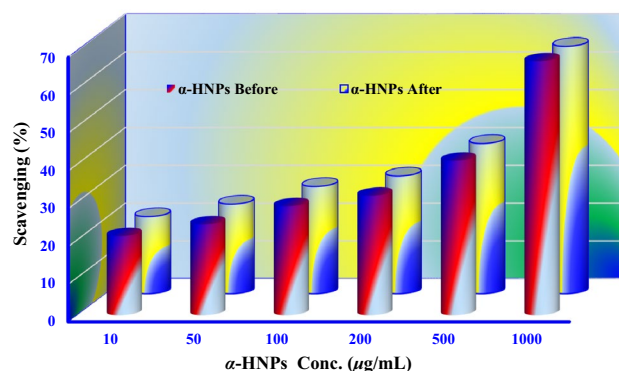


Figure 15. The hydrogen peroxide scavenging effect via α -HNPs before and after Cefotaxime photocatalytic degradation.

were almost not affected at such a low concentration of 100 $\mu\text{g/ml}$. These experiments confirmed the potential application of the biosynthesized *Cfm*@ α -HNPs as a promising anti-proliferative agent.

Hydrogen peroxide scavenging (H_2O_2) assay. In the industrial process, there some properties should be available in the catalyst as the stability of photocatalytic performance that it is very vital; enhancing catalyst life and durability simplifies operations and lowers total costs. If the catalyst has a short life cycle, it will be useless and ineffective in its photocatalytic role. One of the most effective ways that could be used to estimate the photocatalytic performance of the catalysis is the scavenging assay ability.

The human immune system has a complex composition of natural enzymatic and non-enzymatic antioxidant defenses to overcome the deleterious effects of free radicals and other oxidants. Free radicals are responsible for causing a considerable majority of diseases including ulcerative colitis⁶⁹, Alzheimer's disease⁷⁰, Parkinson's disease⁷¹, atherosclerosis⁷², alcohol-induced liver disease⁷³, cancer⁷⁴, cardiovascular disease⁷⁵, mild cognitive impairment⁷⁶, aging⁷⁷, and neural disorders⁷⁸. Safeguarding against free radicals may be improved by a large intake of dietary antioxidants. Substantial evidence suggests that foods containing antioxidants, and probably antioxidant nutrients, in particular, may be of significant significance in the prevention of disease. Antioxidants may benefit greatly in improving the quality of life by preventing or postponing the onset of degenerative diseases.

Human beings are indirectly exposed to H_2O_2 through the environmental surroundings at about 0.28 mg/kg/day, mainly from leaf crops. Hydrogen peroxide may reach the human body through inhalation of vapor or mist and contact with the eyes or skin. H_2O_2 is quickly decomposed into oxygen and water which may create hydroxyl radicals ($\cdot\text{OH}$) that can prompt lipid peroxidation which damages the body's DNA.

Figure 15 shows the hydrogen peroxide scavenging effect of the as-biofabricated α -HNPs before and after the photocatalytic process of *Cfm*. It was very evident from this behavior that the scavenging rate is concentration-dependent. The IC_{50} of hydrogen peroxide scavenging (%) was estimated and it was found to be 635.8 and 665.6 $\mu\text{g/mL}$ of α -HNPs before and after the PCD process of *Cfm* respectively. As we can see the difference between α -HNPs activity before and after the photocatalytic process is less than 5%. This assures our result findings from TEM and FT-IR analysis, where the α -HNPs photocatalytic prosperity did not affect by the *Cfm* degradation process.

Conclusion

In the current study, green bio-fabricated α -HNPs were used in efficient degradation ability to remove the *Cfm* antibiotic drug substance from the contaminated industrial wastewater. The kinetic results of the photocatalytic study manifested that was fitted to the pseudo-first-order kinetic model with R^2 0.992. The optimum *Cfm* photocatalytic conditions were being investigated and they were found to be at a 0.4 g/L loading dose of α -HNPs over 4 h of direct sunlight irradiation at solution pH 10.5. The results revealed the possibility of using the green bio-fabricated α -HNPs as a promising and efficient photocatalytic agent in the treatment of the aquatic contaminated environment with *Cfm*. UV-Vis confirmed that α -HNPs had a direct transition bandgap at 3.78 eV at a maximum absorption wavelength of 362 nm. High stability of the bio-fabricated α -HNPs suspension (-68.6 mV) using zeta potential was realized. XRD, TEM, SEM, EDX, and FT-IR analyses were implemented showing synergistic results for the reusability efficiency of α -HNPs to *Cfm* photocatalytic achievement. Promising antibacterial activity of α -HNPs before and after the PCD process of *Cfm* was investigated showing highly potent ability especially against Gram-positive pathogenic issues more than Gram-negative pathogens. Interestingly, *Cfm*@ α -HNPs showed superior anti-proliferative activity as tested by MTT assay and were able to induce apoptosis in MCF7 and HepG2 cell lines as tested by Annexin-V/PI staining using the flow cytometry technique. Hydrogen peroxide scavenging activity was conducted showing a moderated effect where the IC_{50} was evaluated and it was found to be 635.8 and 665.6 $\mu\text{g/mL}$ of α -HNPs before and after the PCD process of *Cfm* respectively.

Data availability

The data used to support the findings of this study are included in the article.

Received: 5 April 2022; Accepted: 15 June 2022

Published online: 13 July 2022

References

- Al-Hakkani, M. F., Gouda, G. A., Hassan, S. H. A., Mohamed, M. M. A. & Nagiub, A. M. Cefixime wastewater management via bioengineered Hematite nanoparticles and the in-vitro synergetic potential multifunction activities of Cefixime@Hematite nano-system. *Surf. Interfaces* **30**, 101877 (2022).
- Al-Hakkani, M. F., Gouda, G. A. & Hassan, S. H. A. A review of green methods for phytofabrication of hematite (α -Fe₂O₃) nanoparticles and their characterization, properties, and applications. *Heliyon* **7**, e05806 (2021).
- Al-Hakkani, M. F., Hassan, S. H. A., Saddik, M. S., El-Mokhtar, M. A. & Al-Shelkamy, S. A. Bioengineering, characterization, and biological activities of C@Cu₂O@Cu nanocomposite based-mediated the *Vicia faba* seeds aqueous extract. *J. Mater. Res. Technol.* **14**, 1998–2016 (2021).
- Kolpin, D. W. *et al.* Pharmaceuticals, hormones, and other organic wastewater contaminants in US streams, 1999–2000: A national reconnaissance. *Environ. Sci. Technol.* **36**, 1202–1211 (2002).
- Stackelberg, P. E. *et al.* Persistence of pharmaceutical compounds and other organic wastewater contaminants in a conventional drinking-water-treatment plant. *Sci. Total Environ.* **329**, 99–113 (2004).
- Pandiarajan, A., Kamaraj, R. & Vasudevan, S. Enhanced removal of cephalosporin based antibiotics (CBA) from water by one-pot electrosynthesized Mg(OH)₂: A combined theoretical and experimental study to pilot scale. *New J. Chem.* **41**, 4518–4530 (2017).
- Anderson, P. D. *et al.* Screening analysis of human pharmaceutical compounds in US surface waters. *Environ. Sci. Technol.* **38**, 838–849 (2004).
- Tran, N. H., Chen, H., Reinhard, M., Mao, F. & Gin, K.Y.-H. Occurrence and removal of multiple classes of antibiotics and antimicrobial agents in biological wastewater treatment processes. *Water Res.* **104**, 461–472 (2016).
- Rabiet, M. *et al.* Consequences of treated water recycling as regards pharmaceuticals and drugs in surface and ground waters of a medium-sized Mediterranean catchment. *Environ. Sci. Technol.* **40**, 5282–5288 (2006).
- Liu, P., Zhang, H., Feng, Y., Yang, F. & Zhang, J. Removal of trace antibiotics from wastewater: A systematic study of nanofiltration combined with ozone-based advanced oxidation processes. *Chem. Eng. J.* **240**, 211–220 (2014).
- Nikolaou, A., Meric, S. & Fatta, D. Occurrence patterns of pharmaceuticals in water and wastewater environments. *Anal. Bioanal. Chem.* **387**, 1225–1234 (2007).
- Luo, X., Hao, T., Yue, L., Hong, G., Lu, Y., Azithromycin wastewater treatment with la doping titanium dioxide/active carbon composites. In *4th International Conference on Sensors, Measurement and Intelligent Materials*, 861–870 (2016).
- Akmehtmet Balcioğlu, I. & Ötker, M. Treatment of pharmaceutical wastewater containing antibiotics by O₃ and O₃/H₂O₂ processes. *Chemosphere* **50**, 85–95 (2003).
- Guardabassi, L., Petersen, A., Olsen, J. E. & Dalsgaard, A. Antibiotic resistance in *Acinetobacter* spp. isolated from sewers receiving waste effluent from a hospital and a pharmaceutical plant. *Appl. Environ. Microbiol.* **64**, 3499–3502 (1998).
- Leung, H. W. *et al.* Distribution, fate and risk assessment of antibiotics in sewage treatment plants in Hong Kong, South China. *Environ. Int.* **42**, 1–9 (2012).
- Koczura, R. *et al.* Antimicrobial resistance of integron-harboring *Escherichia coli* isolates from clinical samples, wastewater treatment plant and river water. *Sci. Total Environ.* **414**, 680–685 (2012).
- Batt, A. L., Kim, S. & Aga, D. S. Comparison of the occurrence of antibiotics in four full-scale wastewater treatment plants with varying designs and operations. *Chemosphere* **68**, 428–435 (2007).
- Addamo, M. *et al.* Removal of drugs in aqueous systems by photoassisted degradation. *J. Appl. Electrochem.* **35**, 765–774 (2005).
- Wang, Y. *et al.* Degradation of tetracycline in aqueous media by ozonation in an internal loop-lift reactor. *J. Hazard. Mater.* **192**, 35–43 (2011).
- Homem, V. & Santos, L. Degradation and removal methods of antibiotics from aqueous matrices—A review. *J. Environ. Manag.* **92**, 2304–2347 (2011).
- Al-Hakkani, M. F. HPLC analytical method validation for determination of Cefotaxime in the bulk and finished pharmaceutical dosage form. *Sustain. Chem. Eng.* **2020**, 33–42 (2020).
- Dou, M., Wang, J., Gao, B., Xu, C. & Yang, F. Photocatalytic difference of amoxicillin and cefotaxime under visible light by mesoporous g-C₃N₄: Mechanism, degradation pathway and DFT calculation. *Chem. Eng. J.* **383**, 123134 (2020).
- Rodríguez-Mozaz, S. *et al.* Occurrence of antibiotics and antibiotic resistance genes in hospital and urban wastewaters and their impact on the receiving river. *Water Res.* **69**, 234–242 (2015).
- Gulkowska, A. *et al.* Removal of antibiotics from wastewater by sewage treatment facilities in Hong Kong and Shenzhen, China. *Water Res.* **42**, 395–403 (2008).
- Gros, M., Rodríguez-Mozaz, S. & Barceló, D. Rapid analysis of multiclass antibiotic residues and some of their metabolites in hospital, urban wastewater and river water by ultra-high-performance liquid chromatography coupled to quadrupole-linear ion trap tandem mass spectrometry. *J. Chromatogr. A* **1292**, 173–188 (2013).
- León, D. E., Zúñiga-Benítez, H., Peñuela, G. A. & Mansilla, H. D. Photocatalytic removal of the antibiotic cefotaxime on TiO₂ and ZnO suspensions under simulated sunlight radiation. *Water Air Soil Pollut.* **228**, 1–12 (2017).
- Méndez-Díaz, J. *et al.* Kinetic study of the adsorption of nitroimidazole antibiotics on activated carbons in aqueous phase. *J. Colloid Interface Sci.* **345**, 481–490 (2010).
- Radjenović, J., Petrović, M., Ventura, F. & Barceló, D. Rejection of pharmaceuticals in nanofiltration and reverse osmosis membrane drinking water treatment. *Water Res.* **42**, 3601–3610 (2008).
- Adams, C., Wang, Y., Loftin, K. & Meyer, M. Removal of antibiotics from surface and distilled water in conventional water treatment processes. *J. Environ. Eng.* **128**, 253–260 (2002).
- Elmolla, E. S. & Chaudhuri, M. Photocatalytic degradation of amoxicillin, ampicillin and cloxacillin antibiotics in aqueous solution using UV/TiO₂ and UV/H₂O₂/TiO₂ photocatalysis. *Desalination* **252**, 46–52 (2010).
- Martínez-Huitle, C. A. & Ferro, S. Electrochemical oxidation of organic pollutants for the wastewater treatment: Direct and indirect processes. *Chem. Soc. Rev.* **35**, 1324–1340 (2006).
- Gutiérrez, D. J. R., Mathews, N. R. & Martínez, S. S. Photocatalytic activity enhancement of TiO₂ thin films with silver doping under visible light. *J. Photochem. Photobiol. A* **262**, 57–63 (2013).
- Al-Hakkani, M. F. Biogenic copper nanoparticles and their applications: A review. *SN Appl. Sci.* **2**, 505 (2020).
- Saddik, M. S. *et al.* Novel green biosynthesis of 5-fluorouracil chromium nanoparticles using *Harpullia pendula* extract for treatment of colorectal cancer. *Pharmaceutics* **13**, 226 (2021).
- Saddik, M. S. *et al.* Biosynthesis, characterization, and wound-healing activity of phenytoin-loaded Copper nanoparticles. *AAPS PharmSciTech* **21**, 1–12 (2020).
- Al-Hakkani, M. F., Gouda, G. A., Hassan, S. H. A. & Nagiub, A. M. *Echinacea purpurea* mediated hematite nanoparticles (α -HNPs) biofabrication, characterization, physicochemical properties, and its in-vitro biocompatibility evaluation. *Surf. Interfaces* **24**, 101113 (2021).
- Saddik, M. S. *et al.* Tailoring of novel azithromycin-loaded zinc oxide nanoparticles for wound healing. *Pharmaceutics* **14**, 111 (2022).

38. Mousavi, M. *et al.* In-situ construction of ZnO/Sb₂MoO₆ nano-heterostructure for efficient visible-light photocatalytic conversion of N₂ to NH₃. *Surf. Interfaces* **30**, 101844 (2022).
39. Pascariu, P. *et al.* Cu/TiO₂ composite nanofibers with improved photocatalytic performance under UV and UV-visible light irradiation. *Surf. Interfaces* **28**, 101644 (2022).
40. Ph., E., Cefotaxime Sodium monograph (0989) related substances, 7th edition, 1–6 (2013).
41. Al-Hakkani, M. F. Forced degradation study with a developed and validated RP-HPLC method for determination of cefpodoxime proxetil in the bulk and finished pharmaceutical products. *J. Iran. Chem. Soc.* **16**, 1571–1578 (2019).
42. Al-Hakkani, M. F. Guideline of inductively coupled plasma mass spectrometry “ICP–MS”: Fundamentals, practices, determination of the limits, quality control, and method validation parameters. *SN Appl. Sci.* **1**, 791 (2019).
43. Al-Hakkani, M. F. A rapid, developed and validated RP-HPLC method for determination of azithromycin. *SN Appl. Sci.* **1**, 222 (2019).
44. Al-Hakkani, M. F., Gouda, G. A., Hassan, S. H. A., Farghaly, O. A. & Mohamed, M. M. A. Fully investigation of RP-HPLC analytical method validation parameters for determination of Cefixime traces in the different pharmaceutical dosage forms and urine analysis. *Acta Pharm. Sci.* **59**, 97–111 (2021).
45. Lopez-Alvarez, B., Torres-Palma, R. A. & Peñuela, G. Solar photocatalytic treatment of carbofuran at lab and pilot scale: effect of classical parameters, evaluation of the toxicity and analysis of organic by-products. *J. Hazard. Mater.* **191**, 196–203 (2011).
46. Magaldi, S. *et al.* Well diffusion for antifungal susceptibility testing. *Int. J. Infect. Dis.* **8**, 39–45 (2004).
47. Ruch, R. J., Cheng, S.-J. & Klaunig, J. E. Prevention of cytotoxicity and inhibition of intercellular communication by antioxidant catechins isolated from Chinese green tea. *Carcinogen* **10**, 1003–1008 (1989).
48. Šojić, D. V., Anderluh, V. B., Orčić, D. Z. & Abramović, B. F. Photodegradation of clopyralid in TiO₂ suspensions: Identification of intermediates and reaction pathways. *J. Hazard. Mater.* **168**, 94–101 (2009).
49. Lin, Y., Ferronato, C., Deng, N. & Chovelon, J.-M. Study of benzylparaben photocatalytic degradation by TiO₂. *Appl. Catal. B* **104**, 353–360 (2011).
50. León, D. E., Zúñiga-Benítez, H., Peñuela, G. A. & Mansilla, H. D. Photocatalytic removal of the antibiotic cefotaxime on TiO₂ and ZnO suspensions under simulated sunlight radiation. *Water Air Soil Pollut.* **228**, 361 (2017).
51. Reza, K. M., Kurny, A. S. W. & Gulshan, F. Parameters affecting the photocatalytic degradation of dyes using TiO₂: A review. *Appl. Water. Sci.* **7**, 1569–1578 (2017).
52. Harshiny, M., Iswarya, C. N. & Matheswaran, M. Biogenic synthesis of iron nanoparticles using *Amaranthus dubius* leaf extract as a reducing agent. *Powder Technol.* **286**, 744–749 (2015).
53. Basavegowda, N., Mishra, K. & Lee, Y. R. Synthesis, characterization, and catalytic applications of hematite (α -Fe₂O₃) nanoparticles as reusable nanocatalyst. *Adv. Nat. Sci. Nanosci. Nanotechnol.* **8**, 025017 (2017).
54. Alagiri, M. & Hamid, S. B. A. Green synthesis of α -Fe₂O₃ nanoparticles for photocatalytic application. *J. Mater. Sci. Mater. Electron.* **25**, 3572–3577 (2014).
55. Bishnoi, S., Kumar, A. & Selvaraj, R. Facile synthesis of magnetic iron oxide nanoparticles using inedible *Cynometra ramiflora* fruit extract waste and their photocatalytic degradation of methylene blue dye. *Mater. Res. Bull.* **97**, 121–127 (2018).
56. Bibi, I. *et al.* Green synthesis of iron oxide nanoparticles using pomegranate seeds extract and photocatalytic activity evaluation for the degradation of textile dye. *J. Mater. Res. Technol.* **8**, 6115–6124 (2019).
57. Ali, H. R., Nassar, H. N. & El-Gendy, N. S. Green synthesis of α -Fe₂O₃ using *Citrus reticulatum* peels extract and water decontamination from different organic pollutants. *Energy Sources Part A* **39**, 1425–1434 (2017).
58. Groiss, S., Selvaraj, R., Varadavenkatesan, T. & Vinayagam, R. Structural characterization, antibacterial and catalytic effect of iron oxide nanoparticles synthesised using the leaf extract of *Cynometra ramiflora*. *J. Mol. Struct.* **1128**, 572–578 (2017).
59. Bhuiyan, M. S. H. *et al.* Green synthesis of iron oxide nanoparticle using *Carica papaya* leaf extract: Application for photocatalytic degradation of remazol yellow RR dye and antibacterial activity. *Heliyon* **6**, e04603 (2020).
60. Rajiv, P., Bavadharani, B., Kumar, M. N. & Vanathi, P. Synthesis and characterization of biogenic iron oxide nanoparticles using green chemistry approach and evaluating their biological activities. *Biocatal. Agric. Biotechnol.* **12**, 45–49 (2017).
61. Sharma, D. *et al.* Biosynthesis of hematite nanoparticles using *Rheum emodi* and their antimicrobial and anticancerous effects in vitro. *J. Photochem. Photobiol. B* **206**, 111841 (2020).
62. Saddik, M. S., Mohamed, E. & Elmahdy, M. M. Preparation and characterization of niosomal carrier system of hydrophilic drug (methylene blue) for photodynamic therapy. *Lat. Am. J. Pharm* **39**, 561–569 (2020).
63. El-Mahdy, M., Mohamed, E.-E.M., Saddik, M. S., Ali, M. F. & El-Sayed, A. M. Formulation and clinical evaluation of niosomal methylene blue for successful treatment of acne. *J. Adv. Biomed. Pharm. Sci.* **3**, 116–126 (2020).
64. Pallela, P. N. V. K. *et al.* Antibacterial efficacy of green synthesized α -Fe₂O₃ nanoparticles using *Sida cordifolia* plant extract. *Heliyon* **5**, e02765 (2019).
65. Jegadeesan, G. B., Srimathi, K., Srinivas, N. S., Manishkanna, S. & Vignesh, D. Green synthesis of iron oxide nanoparticles using *Terminalia bellirica* and *Moringa oleifera* fruit and leaf extracts: Antioxidant, antibacterial and thermoacoustic properties. *Biocatal. Agric. Biotechnol.* **21**, 101354 (2019).
66. Alam, T. *et al.* Biogenic synthesis of iron oxide nanoparticles via *Skimmia laureola* and their antibacterial efficacy against bacterial wilt pathogen *Ralstonia solanacearum*. *Mater. Sci. Eng. C* **98**, 101–108 (2019).
67. Chauhan, S. & Upadhyay, L. S. B. Biosynthesis of iron oxide nanoparticles using plant derivatives of *Lawsonia inermis* (Henna) and its surface modification for biomedical application. *Nanotechnol. Environ. Eng.* **4**, 8 (2019).
68. Jamzad, M. & Bidkorpeh, M. K. Green synthesis of iron oxide nanoparticles by the aqueous extract of *Laurus nobilis* L. leaves and evaluation of the antimicrobial activity. *J. Nanostruct. Chem.* **10**, 1–9 (2020).
69. Ramakrishna, B., Varghese, R., Jayakumar, S., Mathan, M. & Balasubramanian, K. Circulating antioxidants in ulcerative colitis and their relationship to disease severity and activity. *J. Gastroenterol. Hepatol.* **12**, 490–494 (1997).
70. Smith, M. A., Rottkamp, C. A., Nunomura, A., Raina, A. K. & Perry, G. Oxidative stress in Alzheimer’s disease. *Biochim. Biophys. Acta* **1502**, 139–144 (2000).
71. Bolton, J. L., Trush, M. A., Penning, T. M., Dryhurst, G. & Monks, T. J. Role of Quinones in toxicology. *Chem. Res. Toxicol.* **13**, 135–160 (2000).
72. Upston, J. M., Kritharides, L. & Stocker, R. The role of vitamin E in atherosclerosis. *Prog. Lipid Res.* **42**, 405–422 (2003).
73. Arteel, G. E. Oxidants and antioxidants in alcohol-induced liver disease. *Gastroenterol.* **124**, 778–790 (2003).
74. Kinnula, V. L. & Crapo, J. D. Superoxide dismutases in malignant cells and human tumors. *Free Radic. Biol. Med.* **36**, 718–744 (2004).
75. Singh, U. & Jialal, I. Oxidative stress and atherosclerosis. *Pathophysiology* **13**, 129–142 (2006).
76. Guidi, I. *et al.* Oxidative imbalance in patients with mild cognitive impairment and Alzheimer’s disease. *Neurobiol. Aging* **27**, 262–269 (2006).
77. Hyun, D.-H., Hernandez, J. O., Mattson, M. P. & de Cabo, R. The plasma membrane redox system in aging. *Aging Res. Rev.* **5**, 209–220 (2006).
78. Sas, K., Robotka, H., Toldi, J. & Vécsei, L. Mitochondria, metabolic disturbances, oxidative stress and the kynurenine system, with focus on neurodegenerative disorders. *J. Neurol. Sci.* **257**, 221–239 (2007).

Acknowledgements

This paper is based upon work supported by Science, Technology & Innovation Funding Authority (STDF) under Grant No. (44593).

Author contributions

M.F.A.: Conceptualization, Methodology, Software, Data curation, Writing – original draft, Visualization, Investigation, Validation, Writing – review & editing. G.A.G.: Conceptualization, Methodology, Software, Supervision. S.H.A.H.: Conceptualization, Methodology, Software, Supervision. M.S.S.: Methodology, Software, Data curation, Writing – original draft, Visualization, Investigation, Validation, Writing – review & editing. M.A.E.: Methodology, Software, Data curation, Writing – original draft, Visualization, Investigation, Validation, Writing – review & editing. M.A.I.: Methodology, Software, Data curation, Writing – original draft, Visualization, Investigation, Validation, Writing – review & editing. M.M.A.M.: Conceptualization, Supervision. A.M.N.: Conceptualization, Supervision.

Funding

Open access funding provided by The Science, Technology & Innovation Funding Authority (STDF) in cooperation with The Egyptian Knowledge Bank (EKB).

Competing interests

The authors declare no competing interests.

Additional information

Supplementary Information The online version contains supplementary material available at <https://doi.org/10.1038/s41598-022-14922-3>.

Correspondence and requests for materials should be addressed to M.F.A.-H.

Reprints and permissions information is available at www.nature.com/reprints.

Publisher's note Springer Nature remains neutral with regard to jurisdictional claims in published maps and institutional affiliations.



Open Access This article is licensed under a Creative Commons Attribution 4.0 International License, which permits use, sharing, adaptation, distribution and reproduction in any medium or format, as long as you give appropriate credit to the original author(s) and the source, provide a link to the Creative Commons licence, and indicate if changes were made. The images or other third party material in this article are included in the article's Creative Commons licence, unless indicated otherwise in a credit line to the material. If material is not included in the article's Creative Commons licence and your intended use is not permitted by statutory regulation or exceeds the permitted use, you will need to obtain permission directly from the copyright holder. To view a copy of this licence, visit <http://creativecommons.org/licenses/by/4.0/>.

© The Author(s) 2022